J|A|C|S
ARTICLES
Published on Web 12/07/2002

Measurements of Electron-Transfer Rates of Charge-Storage Molecular Monolayers on Si(100). Toward Hybrid Molecular/Semiconductor Information Storage Devices

Kristian M. Roth,[†] Amir A. Yasseri,[†] Zhiming Liu,[†] Rajeev B. Dabke,[†] Vladimir Malinovskii,[‡] Karl-Heinz Schweikart,[‡] Lianhe Yu,[‡] Hugo Tiznado,[†] Francisco Zaera,*[,†] Jonathan S. Lindsey,*[,‡] Werner G. Kuhr,*[,†] and David F. Bocian*[,†]

Contribution from the Department of Chemistry, University of California, Riverside, California 92521-0403, and Department of Chemistry, North Carolina State University, Raleigh, North Carolina 27695-8204

Received September 10, 2002; E-mail: david.bocian@ucr.edu

Abstract: Redox kinetics were measured for two electroactive molecules attached to Si(100) surfaces, a ferrocene (**Fc-BzOH**) and a Zn(II) trimesitylporphyrin (**Por-BzOH**). Each molecule was derivatized with a benzyl alcohol linker for attachment to the Si surface via the formation of a Si−O bond. A complete protocol was developed for the preparation of stable Si(100) surfaces derivatized with the electroactive molecules. The redox-kinetic measurements were performed on the resulting **Fc-BzOH** and **Por-BzOH** monolayers to probe (1) the rate of electron transfer (k^0) for oxidation in the presence of applied potentials and (2) the rate of charge dissipation after the applied potential is disconnected (in the form of a charge-retention half-life $t_{1/2}$). The k^0 values for the two types of monolayers were found to be similar to one another as were the $t_{1/2}$ values. Perhaps more importantly, the electron-transfer rates for both the **Fc-BzOH** and the **Por-BzOH** monolayers differ from the charge-dissipation rates by ~6 orders of magnitude and are strongly dependent on the surface concentration of the electroactive species. For the **Por-BzOH** monolayers on Si(100), the k^0 and $t_{1/2}$ values and their trends as a function of surface coverage were determined to be similar to those previously measured for the analogous thiol-derivatized molecule assembled on Au(111). In contrast, the **Fc-BzOH** monolayers on Si(100) were found to exhibit much slower electron-transfer and charge-dissipation rates than those in the corresponding thiol-Au(111) case. Two alternative hypotheses are advanced to explain both the diminution in rates with increased surface coverage and the contrasting behavior with the analogous thiols on Au, one based on space-charge effects at the monolayer−solution interface, and a second relying on changes in distance of the redox centers from the surface as modulated by the orientation of the linking chains. Collectively, the ability to prepare and study stable, electroactive molecular media on Si(100) is likely to be key in the development of hybrid molecular/semiconductor devices.

I. Introduction

Semiconductors have served as the basic materials for constructing electronic devices for the past 50 years. Semiconductor technology continues to extend into regimes previously thought inaccessible. Despite this progress, it is uncertain whether devices that rely on the bulk properties of materials will retain the required characteristics to function when feature sizes ultimately reach nanoscale dimensions. As a consequence, there has been an intense interest in developing molecular-based electronic materials for use in both memory architectures and circuit elements.[1−6] Toward this goal, we have been engaged in a program aimed at constructing devices that use the properties of molecules to store information.[7−10] In our general approach, a collection of redox-active molecules attached to an electroactive surface serves as the active storage medium, and information is stored in the discrete redox states of the molecules. Porphyrins were chosen as the information storage medium because they exhibit a number of key properties:[7−16]

[†] University of California.
[‡] North Carolina State University.

(1) Collier, C. P.; Jeppesen, J. O.; Luo, Y.; Perkins, J.; Wong, E. W.; Heath, J. R.; Stoddart, J. F. *J. Am. Chem. Soc.* **2001**, *123*, 12632−12641.
(2) Collier, C. P.; Ma, B.; Wong, E. W.; Heath, J. R.; Wudl, F. *ChemPhysChem* **2002**, *3*, 458−461.
(3) Huang, Y.; Duan, X.; Cui, Y.; Lauhon, L. J.; Kim, K.-H.; Lieber, C. M. *Science* **2001**, *294*, 1313−1317.
(4) Duan, X.; Huang, Y.; Lieber, C. M. *Nano Lett.* **2002**, *2*, 487−490.
(5) Chen, J.; Reed, M. A. *Chem. Phys.* **2002**, *281*, 127−145.
(6) Chen, J.; Wang, W.; Klemic, J.; Reed, M. A.; Axelrod, B. W.; Kaschak, D. M.; Rawlett, A. M.; Price, D. W.; Dirk, S. M.; Tour, J. M.; Grubisha, D. S.; Bennett, D. W. *Ann. N.Y. Acad. Sci.* **2002**, *960*, 69−99.
(7) Roth, K. M.; Dontha, N.; Dabke, R. B.; Gryko, D. T.; Clausen, C.; Lindsey, J. S.; Bocian, D. F.; Kuhr, W. G. *J. Vac. Sci. Technol., B* **2000**, *18*, 2359−2364.
(8) Roth, K. M.; Dabke, R. B.; Liu, Z.; Yasseri, A. A.; Gryko, D. T.; Clausen, C.; Lindsey, J. S.; Bocian, D. F.; Kuhr, W. G. *ACS Symp. Series* **2002**, *844*.
(9) Gryko, D.; Li, J.; Diers, J. R.; Roth, K. M.; Bocian, D. F.; Kuhr, W. G.; Lindsey, J. S. *J. Mater. Chem.* **2001**, *11*, 1162−1180.
(10) Roth, K. M.; Lindsey, J. S.; Bocian, D. F.; Kuhr, W. G. *Langmuir* **2002**, *18*, 4030−4040.
(11) Gryko, D. T.; Clausen, C.; Roth, K. M.; Dontha, N.; Bocian, D. F.; Kuhr, W. G.; Lindsey, J. S. *J. Org. Chem.* **2000**, *65*, 7345−7355.

(1) they form π-cation radicals that are relatively stable under ambient conditions, facilitating real-world applications; (2) they exhibit multiple cationic states that are accessible at relatively low potentials, affording multibit information storage with low power consumption; and (3) they are capable of storing charge for extended periods, up to tens of minutes, in the absence of applied potential, further diminishing power consumption and significantly attenuating the refresh rates required in a memory device.

Our past studies have focused primarily on thiol-derivatized porphyrin-based self-assembled monolayers (SAMs) on Au surfaces. During the course of that research, a large number (100+) of molecules were prepared bearing a variety of thiol-terminated organic linkers.[11−16] The charge-storage capabilities of the molecules have been investigated as a function of both porphyrin architecture and organic linker type. More recently, the electron-transfer rates in the presence of an applied potential were determined for a representative subset of these porphyrin SAMs, and a correlation between those rates and the charge-dissipation rates in the absence of any applied potential was identified.[17] [We use the term "charge dissipation" to distinguish this process from the reverse of the oxidative electron-transfer reaction, because the former process is passive (potential not applied), whereas the latter is active (potential applied).] Indeed, these studies revealed that the kinetics of the two processes are directly related. In particular, porphyrin SAMs that exhibit fast electron transfer also exhibit relatively rapid charge dissipation, that is, short charge-retention times, and vice versa. In addition, the rates of both processes depend on the surface concentration of the electroactive species: more densely packed SAMs exhibit slower kinetics for both processes. The most surprising aspect of the kinetic behavior of these systems is that the electron-transfer rates (10^4-10^5 s^{-1}) for the porphyrin SAMs on Au are typically 6 orders of magnitude faster than the charge-dissipation rates ($10^{-1}-10^{-3}$ s^{-1}).

Our earlier studies of thiol-derivatized porphyrin SAMs on Au have served as a fertile test-bed for benchmarking the characteristics of these molecules for molecular-based information storage. However, the first generation of practical molecular-based devices is likely to embody some type of hybrid molecular/semiconductor architecture, where the molecular material would be attached to a semiconductor rather than to a metal electrode. The implementation of hybrid molecular/semiconductor architectures as a transition technology offers a number of possible advantages over molecular assemblies on metals: (1) the technology for handling semiconductor materials such as Si wafers is well established, it is relatively easy to obtain atomically flat crystalline Si, and devices on Si are relatively easy to pattern; (2) the electronic properties of the Si surface, such as its conductivity, can be manipulated by altering the dopant type (*p* or *n*) or concentration; and (3) bonds such as Si−C or Si−O, which are likely links between Si surfaces and organic adsorbates, are much stronger (Si−C, ∼76 kcal mol^{-1}; Si−O, ∼108 kcal mol^{-1})[18] than bonds such as Au−S (∼45 kcal mol^{-1}).[19] Collectively, these features indicate that hybrid molecular/semiconductor constructs should be easier to manufacture, may be prepared with more diverse electrical characteristics, and will most likely exhibit better stability than molecular/metal architectures.

The implementation of molecular/semiconductor architectures also presents significant challenges. For one, there is the issue of the chemistry of attachment of the organic species to the Si surface. Because Si−C and Si−O are relatively strong covalent bonds, the anchoring chemistry needs to be more aggressive than the more facile process of self-assembly of thiols on Au. Toward this goal, there have been a number of recent studies exploring the attachment of organic molecules to Si surfaces.[20] The routes examined include (1) hydrosilylation reactions involving alkenes and alkynes on hydride-passivated Si,[21−23] (2) the reaction of organosilanes and amines with chloride-terminated or neat Si surfaces,[24] (3) the use of alkyl Grignard or alkyllithium reagents,[25,26] (4) cycloaddition reactions involving butadienes,[27,28] and (5) the thermal reaction of alcohols and aldehydes with hydride-passivated Si.[23,24,29−33] A second issue concerns the reactivity of the Si surface. Activated Si surfaces, unlike those of Au, are susceptible to oxidative damage. In particular, the Si surface may contain dangling bonds, which may serve as initiation sites for reactions leading to surface deterioration. Accordingly, issues such as the passivation of the remaining exposed Si surface after attachment of the molecular species of interest are potentially much more important than they are for relatively inert metal electrodes.

As a first step toward the goal of developing hybrid molecular/semiconductor information storage devices, we have measured both electron-transfer rates and charge-retention times for two prototypical electroactive molecules attached to single-crystal Si surfaces. The electroactive molecules used in this study were a ferrocene and a Zn(II) trimesitylporphyrin, each derivatized with a benzyl alcohol linker for attachment to the Si surface via the formation of a Si−O bond. The structures of the two molecules (designated **Fc-BzOH** and **Por-BzOH**) are shown in Chart 1. To our knowledge, there have been no previous studies on the electron-transfer rates of redox-active molecular

(12) Gryko, D. T.; Zhao, F.; Yasseri, A. A.; Roth, K. M.; Bocian, D. F.; Kuhr, W. G.; Lindsey, J. S. *J. Org. Chem.* **2000**, *65*, 7356−7362.
(13) Clausen, C.; Gryko, D. T.; Dabke, R. B.; Dontha, N.; Bocian, D. F.; Kuhr, W. G.; Lindsey, J. S. *J. Org. Chem.* **2000**, *65*, 7363−7370.
(14) Clausen, C.; Gryko, D. T.; Yasseri, A. A.; Diers, J. R.; Bocian, D. F.; Kuhr, W. G.; Lindsey, J. S. *J. Org. Chem.* **2000**, *65*, 7371−7378.
(15) Li, J.; Gryko, D.; Dabke, R. B.; Diers, J. R.; Bocian, D. F.; Kuhr, W. G.; Lindsey, J. S. *J. Org. Chem.* **2000**, *65*, 7379−7390.
(16) Schweikart, K.-H.; Malinovskii, V. L.; Diers, J. R.; Yasseri, A. A.; Bocian, D. F.; Kuhr, W. G.; Lindsey, J. S. *J. Mater. Chem.* **2002**, *12*, 808−828.
(17) Roth, K. M.; Gryko, D. T.; Clausen, C.; Li, J.; Lindsey, J. S.; Kuhr, W. G.; Bocian, D. F. *J. Phys. Chem. B* **2002**, *106*, 8639−8648.
(18) Choi, C. H.; Liu, D.-J.; Evans, J. W.; Gordon, M. S. *J. Am. Chem. Soc.* **2002**, *124*, 8730−8740.
(19) Dubois, L. H.; Nuzzo, R. G. *Annu. Rev. Phys. Chem.* **1992**, *43*, 437−463.
(20) Song, J. H.; Sailor, M. J. *Comments Inorg. Chem.* **1999**, *21*, 69−84.
(21) Hovis, J. S.; Hamers, R. J. *J. Phys. Chem. B* **1998**, *102*, 687−692.
(22) Hovis, J. S.; Lee, S.; Liu, H.; Hamers, R. J. *J. Vac. Sci. Technol., B* **1997**, *15*, 1153−1158.
(23) Bateman, J. E.; Eagling, R. D.; Horrocks, B. R.; Houlton, A. *J. Phys. Chem. B* **2000**, *104*, 5557−5565.
(24) Barrelet, C. J.; Robinson, D. B.; Cheng, J.; Hunt, T. P.; Quate, C. F.; Chidsey, C. E. D. *Langmuir* **2001**, *17*, 3460−3465.
(25) Bansal, A.; Li, X.; Lauermann, I.; Lewis, N. S.; Yi, S. I.; Weinberg, W. H. *J. Am. Chem. Soc.* **1996**, *118*, 7225−7226.
(26) Yu, H.-Z.; Morin, S.; Wayner, D. D. M.; Allongue, P.; de Villeneuve, C. H. *J. Phys. Chem. B* **2000**, *104*, 11157−11161.
(27) Bent, S. F. *Surf. Sci.* **2002**, *500*, 879−903.
(28) Hamers, R. J.; Coulter, S. K.; Ellison, M. D.; Hovis, J. S.; Padowitz, D. F.; Schwartz, M. P.; Greenlief, C. M.; Russell, J. N., Jr. *Acc. Chem. Res.* **2000**, *33*, 617−624.
(29) Boukherroub, R.; Morin, S.; Sharpe, P.; Wayner, D. D. M.; Allongue, P. *Langmuir* **2000**, *16*, 7429−7434.
(30) Zhu, X. Y.; Boiadjiev, V.; Mulder, J. A.; Hsung, R. P.; Major, R. C. *Langmuir* **2000**, *16*, 6766−6772.
(31) Mo, R. T.; Burr, T. A.; Merklin, G. T.; Machuca, F.; Pianetta, P. A.; Kimerling, L. C.; Chiarello, R. P.; Chidsey, C. E. D. *Proc. Electrochem. Soc.* **2000**, *99*−*36*, 545−552.
(32) Cleland, G.; Horrocks, B. R.; Houlton, A. *J. Chem. Soc., Faraday Trans.* **1995**, *91*, 4001−4003.
(33) Kim, N. Y.; Laibinis, P. E. *J. Am. Chem. Soc.* **1997**, *119*, 2297−2298.

Chart 1. Structures of **Fc-BzOH**, **Por-BzOH**, and **BPM**

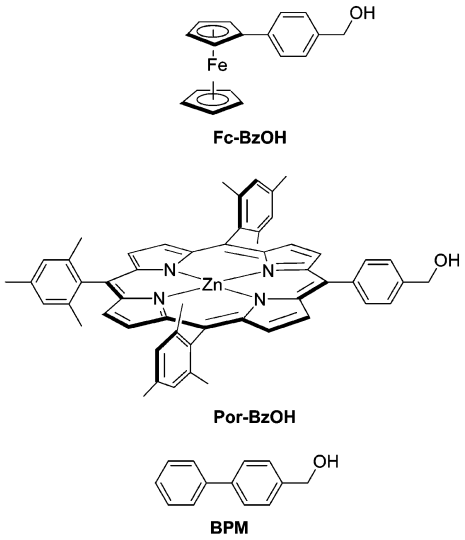

monolayers on Si surfaces (unlike the case of thiol-derivatized redox-active molecules on Au, for which a number of studies have been reported[17,34−40]). Instead, previous studies have focused on the electron-transfer rates of molecules in solution through blocking or inert monolayers on Si surfaces.[41,42] There have also been a few electrochemical (cyclic voltammetry) studies of alcohol-derivatized ferrocenes attached to *n*-type Si surfaces;[43−45] however, because the (positive) redox potential of ferrocene is well above the flat-band potential of the *n*-type Si, those measurements are susceptible to photogenerated carrier effects. To avoid this problem, device-quality high conductivity *p*-type Si(100) was chosen for our studies of the **Fc-BzOH** and **Por-BzOH** monolayers. A preliminary electrochemical, conductance/capacitance study of the **Fc-BzOH** monolayers on this substrate has recently been published.[46]

A number of important advances were made in the studies reported herein. First, a complete protocol was developed for the successful preparation of stable Si(100) surfaces derivatized with electroactive molecules. The molecules of interest were attached via Si−O linkages through the intermediate preparation of hydrogen- and iodine-terminated surfaces. Second, the electrical behavior of those surface layers was fully characterized. As in the case of thiols on Au, it was found that our Si-based devices display electron-transfer rates that are several orders of magnitude faster than their charge-dissipation rates. This is a very desirable property from the standpoint of memory device development, because it implies that the molecular oxidation states can be easily accessed by applying appropriate voltages and preserved for long periods of time once those voltages are removed. Of particular importance was our finding that both electron-transfer and charge-retention rates are primarily controlled by the surface concentration of the active molecules, decreasing by more than an order of magnitude as monolayer saturation is approached. We speculate that such variations may be associated with either space-charge effects at the monolayer−solvent interface or changes in adsorption geometry induced by surface crowding. In any case, this factor, which has been shown to be more important than changes in either the substrate (from Au to Si) or the nature of the surface bonding (Au−S versus Si−O), could be controlled by the use of an inert co-attached species.

The layout of the paper is as follows. We first address the optimization of the process for attaching the molecules to the Si surface. These studies include characterization by both X-ray photoelectron spectroscopy (XPS) and electrochemical methods. We then describe the measurement of the kinetics of electron transfer (in the presence of an applied potential) and charge dissipation (in the absence of any applied potential) for the **Fc-BzOH** and **Por-BzOH** monolayers on Si. Those rates measured here for the Si-based architectures are compared to those observed for SAMs of the analogous thiol-derivatized molecules on Au.

II. Experimental Section

A. Chemicals, Materials, and General Procedures. The syntheses of **Fc-BzOH** and **Por-BzOH** are described in the Supporting Information. 4-Biphenylmethanol (**BPM**) could be obtained commercially or prepared by $NaBH_4$ reduction of 4-biphenylcarboxaldehyde (Aldrich) using standard procedures.

Silicon wafers (Silicon Valley Microelectronics) were purchased as thermally oxidized B-doped Si(100) ($\rho = 0.005-0.1\ \Omega$ cm). The chemicals used in Si microelectrode fabrication were AZ 5214 (positive photoresist, Baker), AZ 400K (photoresist developer, Baker), Baker Aleg-355 (resist stripper, Baker), Nanostrip (Cyantek), HF dip (5:1) (Baker), Buffered Oxide Etch (10:1) (Baker), and Baker Clean JTB-111 (Baker). Ar and N_2 (99.995%) were passed through Drierite (Fisher) and Oxyclear (Supelco) gas purifiers prior to use. Deionized water (from a Milli-Q system) had a $\rho \geq 16$ MΩ cm.

The anhydrous solvents used in the preparation of the monolayers and in the electrochemical measurements, $CHCl_3$ (Aldrich, 99%), benzonitrile (Aldrich, 99%), CH_2Cl_2 (Aldrich, 99.8%), pyridine (Fluka), and propylene carbonate (PC) (Aldrich, 99.7%), were used as received. Iodine (Fisher) was also used as received. The Bu_4NPF_6 (Aldrich) supporting electrolyte was recrystallized three times from methanol (Fisher) and dried at 110 °C under vacuum.

B. Electrode Fabrication. 1. Si(100) Microelectrode. The electrochemical measurements on the monolayers were made using a 100 μm × 100 μm *p*-type Si(100) working microelectrode. A microelectrode was used to ensure that the RC time constant of the electrochemical cell was sufficiently short so that fast kinetic events could be accurately measured. A short cell time constant is also essential for performing the charge-retention measurements described below. The RC time constant of the electrochemical cell constructed using the Si(100) working microelectrode was found to be ∼4 μs by using a potential step function.

The Si(100) microelectrodes were fabricated from an AutoCAD designed negative photomask master (Photo Sciences). The negative

(34) Sikes, H. D.; Smalley, J. F.; Dudek, S. P.; Cook, A. R.; Newton, M. D.; Chidsey, C. E. D.; Feldberg, S. W. *Science* **2001**, *291*, 1519−1523.
(35) Sachs, S. B.; Dudek, S. P.; Hsung, R. P.; Sita, L. R.; Smalley, J. F.; Newton, M. D.; Feldberg, S. W.; Chidsey, C. E. D. *J. Am. Chem. Soc.* **1997**, *119*, 10563−10564.
(36) Forster, R. J.; Faulkner, L. R. *J. Am. Chem. Soc.* **1994**, *116*, 5444−5452.
(37) Forster, R. J.; Faulkner, L. R. *J. Am. Chem. Soc.* **1994**, *116*, 5453−5461.
(38) Finklea, H. O.; Hanshew, D. D. *J. Am. Chem. Soc.* **1992**, *114*, 3173−3181.
(39) Creager, S.; Yu, C. J.; Bamdad, C.; O'Connor, S.; MacLean, T.; Lam, E.; Chong, Y.; Olsen, G. T.; Luo, J.; Gozin, M.; Kayyem, J. F. *J. Am. Chem. Soc.* **1999**, *121*, 1059−1064.
(40) Chidsey, C. E. D. *Science* **1991**, *251*, 919−922.
(41) Cheng, J.; Robinson, D. B.; Cicero, R. L.; Eberspacher, T.; Barrelet, C. J.; Chidsey, C. E. D. *J. Phys. Chem. B* **2001**, *105*, 10900−10904.
(42) Bansal, A.; Lewis, N. S. *J. Phys. Chem. B* **1998**, *102*, 1067−1070.
(43) Fischer, A. B.; Bruce, J. A.; McKay, D. R.; Maciel, G. E.; Wrighton, M. S. *Inorg. Chem.* **1982**, *21*, 1766−1771.
(44) Miller, R. J. D. *Surface Electron-Transfer Processes*; VCH Publishers: New York, 1995.
(45) Bateman, J. E.; Eagling, R. D.; Worrall, D. R.; Horrocks, B. R.; Houlton, A. *Angew. Chem., Int. Ed.* **1998**, *37*, 2683−2685.
(46) Li, Q.; Mathur, G.; Homsi, M.; Surthi, S.; Misra, V.; Malinovskii, V.; Schweikart, K.-H.; Yu, L.; Lindsey, J. S.; Liu, Z.; Dabke, R. B.; Yasseri, A.; Bocian, D. F.; Kuhr, W. G. *Appl. Phys. Lett.* **2002**, *81*, 1494−1496.

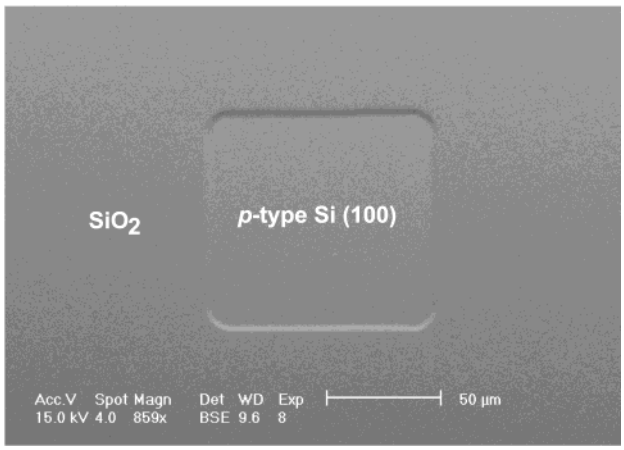

Figure 1. SEM of the Si(100) microelectrode. The electrode surface area is 100 × 100 μm; the microvia depth is 300 nm.

mask contained an array of 74 repeating 36 mm^2 square units arranged into rows and columns spaced 5 mm apart (yielding 74 microelectrodes per wafer). Each unit square contained a 100 × 100 μm ($\pm$1 μm) hole positioned at its center, which defined the microelectrode. Four additional holes positioned on the outer perimeter of each unit square served as guides to facilitate positioning of the microelectrode for the electrochemical experiments.

Presealed thermally oxidized 100 mm diameter wafers were first coated with photoresist (AZ-5214) using a spin coater (3000 rpm, 30 s), and then soft baked at 100 °C for 1 min. The resist film-coated wafers were then aligned with the photomask (Karl Suess MA6 operated in hard contact mode) and exposed to 365 nm UV light. After exposure, the microelectrode pattern was developed (AZ 400 K, 1:4 v/v), rinsed with deionized water, and hard baked at 150 °C for 3 min. Subsequently, the thermally grown oxide overlayer unprotected by the resist was etched to expose the hydride-passivated Si(100) surface. The conditions for the etching process were optimized on larger Si(100) platforms prior to fabrication of the microelectrodes. Hydride passivation was examined both qualitatively by looking at the hydrophobicity characteristics of the surface[47,48] and quantitatively by XPS studies (vide infra). The surface was first isotropically etched using a buffered oxide solution[48] to remove the top ~2800 Å of surface oxide. An etch rate of ~10 Å/s was generally observed for this solution at room temperature. The last ~200 Å of oxide was etched using a 10% HF solution at an etch rate of ~2 Å/s. The etch process yielded a well-defined microvia with a relatively smooth (~5 Å, determined by atomic force microscopy using a Digital Instruments Nanoscope III) hydride-passivated Si(100) surface at the bottom. It should be noted that the use of only neat buffered oxide or NH_4F [49,50] to etch Si(100) results in pronounced surface roughness (~100 Å), which was found to yield inferior molecular attachment to the surface. Finally, resist stripper was used to remove the photoresist, after which the wafer was cut to yield the individual microelectrodes. A scanning electron micrograph (SEM) of a typical microelectrode, obtained using a Philips XL with a backscattering electron detector with an acceleration voltage of 15 keV, is shown in Figure 1. A thin (~30 Å) Au film was sputtered onto the surface to allow for greater contrast between the electrode and the oxidized overlayer.

Prior to use, each microelectrode was precleaned by sonication in Baker-111 clean solution to remove trace metal impurities. Following a deionized water rinse, the samples were immersed in nanostrip solution to eliminate residual organic contaminants. The two-step cleaning procedure resulted in the regrowth of a thin sacrificial native oxide film showing a measured surface roughness of ~5 Å. Removal of residual oxide from the electrode surface was accomplished by immersing the samples in a dilute (1%) HF solution. The solution was sparged with Ar prior to its use to remove dissolved oxygen, because dissolved oxygen has been reported to initiate etch pits on terraces of hydride-passivated Si.[51] The optimum time to remove native oxide from the surface while maintaining the geometric integrity of the microelectrode was found to be 3 min; longer etch times and higher etchant concentrations resulted in overetching due to the absence of photoresist and the isotropic nature of the etchant. The etched microelectrodes were immediately rinsed for 10−40 s with deionized water to remove fluorine from the surface[52] and blown dry with N_2 (99.999%). Once completely dry, the samples were immediately placed into VOC vials (Supelco) and sealed using a septum-fitted cap. Each vial was purged thoroughly with dry Ar for 5 min and heated to 250 °C while maintaining the purge for an additional 5 min. This process removes residual physisorbed water and surface silanol groups.[49] Although oxide growth on HF-treated Si surfaces stored in air has been reported to proceed extremely slowly,[49] we observed that monolayer formation is significantly improved if the microelectrodes are maintained under inert conditions.

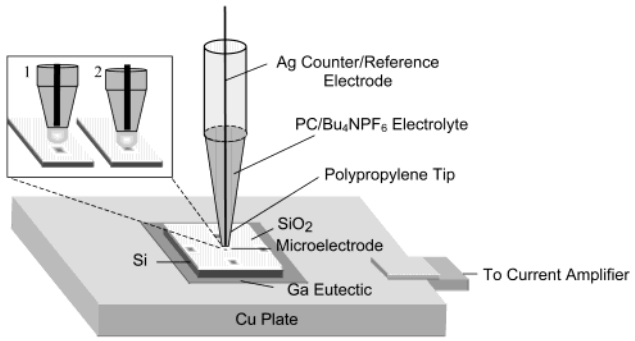

Figure 2. Schematic diagram of the electrochemical cell. The electrode, etched into an ~36 mm^2 section of *p*-type Si(100) wafer, was mounted on to a Cu plate using a Ga eutectic to provide electrical contact through the backside of the wafer. A polypropylene micropipet tip, containing the Ag counter/reference electrode and filled with electrolyte solution, is positioned over the microvia using a micropositioner. Inset: (1) Capillary force maintains the microdrop at the tip of the pipet (~500 μm i.d.) prior to contact with the surface. (2) Contact with the surface fills the microvia with the electrolyte solution.

2. Counter/Reference Electrode. A bare silver wire (Ag/Ag^+) served as the counter/reference electrode. The electrode was prepared by sonicating the Ag wire (Goodfellow) in 7.0 M NH_4OH, rinsing it in deionized water and ethanol, and sonicating it in CH_2Cl_2 containing 1.0 M Bu_4NPF_6. The prepared Ag wire was placed inside a 10 μL polypropylene disposable pipet tip containing ~5 μL of the PC/1.0 M Bu_4NPF_6 electrolyte solution. A schematic diagram of the counter/reference electrode is shown in Figure 2.

C. Monolayer Preparation. A number of approaches were explored to prepare high-quality monolayers of **Fc-BzOH** and **Por-BzOH** on the Si(100) surface. The molecular attachment procedure was refined on larger Si(100) platforms prior to application to the microelectrodes. Certain procedures gave good results under ambient environments, but substantially better results were obtained under inert atmosphere conditions.

Because there have been a number of previous reports on attachment of alcohols to hydride-passivated Si surfaces (via Si−H bond cleavage to form Si−O linkages),[23,24,29,30,32,33] this was the first approach chosen here to attach the **Fc-BzOH** and **Por-BzOH** molecules to our Si(100) surface. However, experiments wherein $CHCl_3$ solutions of the

(47) Grundner, M.; Jacob, H. *Appl. Phys. A* **1986**, *A39*, 73−82.
(48) Graef, D.; Bauer-Mayer, S.; Schnegg, A. *J. Vac. Sci. Technol., A* **1993**, *11*, 940−944.
(49) Graef, D.; Grunder, M.; Schulz, R.; Muehlhoff, L. *J. Appl. Phys.* **1990**, *68*, 5155−5161.
(50) Houston, M. R.; Maboudian, R. *J. Appl. Phys.* **1995**, *78*, 3801−3808.
(51) Wade, C. P.; Chidsey, C. E. D. *Appl. Phys. Lett.* **1997**, *71*, 1679−1681.
(52) Ibach, H.; Bruchmann, H. D.; Wagner, H. *Appl. Phys.* **1982**, *A29*, 113−124.

molecules were layered on the hydride-passivated Si(100) surface at room temperature failed to produce good quality monolayers (as evidenced by poor quality voltammograms), even after extended exposure periods. Subsequently, attachment was attempted at elevated temperatures (70−100 °C for **Fc-BzOH**; 170 °C for **Por-BzOH**) using benzonitrile as the solvent (bp 191 °C). This approach only marginally improved the quality of the monolayers. Next, a strategy was implemented wherein microdrops (∼2 μL) of solution were periodically released onto the heated hydride-passivated Si(100) surface over a period of 3 h. This approach afforded a noticeable improvement in the voltammetric characteristics of both the **Fc-BzOH** and the **Por-BzOH** monolayers. Presumably, the high surface concentration that occurs as the microdrops rapidly evaporate greatly accelerates the kinetics of the surface derivatization reaction. Regardless, the voltammetric characteristics of the monolayers were still deemed less than optimum.

Previous studies have indicated that halide-modified Si surfaces afford superior attachment of organic molecules due to the enhanced lability of the Si−X (X = Cl, Br, I) bond relative to the Si−H bond.[30,31,53−58] The presence of oxidants such as I_2 and Br_2 in alcoholic solutions has also been shown to facilitate Si−O bond formation on Si(100) surfaces.[58] As a consequence, attachment to halide-modified surfaces was explored next.

The hydride-passivated Si(100) surfaces were treated with a saturated solution of I_2 in anhydrous $CHCl_3$. The solutions were sparged with dry Ar in sealed containers and allowed to react with the surface for 10 min under red light (632 nm). The use of red light minimizes photoinduced Si−I bond cleavage.[59] The Si surfaces were then rinsed and sonicated four times in $CHCl_3$ under dry Ar purge in the sealed vials. The conditions for optimizing the iodide surface concentration, determined using XPS (vide infra), were again refined on larger Si(100) platforms prior to use on the microelectrodes.

The **Fc-BzOH** and **Por-BzOH** monolayers were prepared on the iodide-modified Si(100) microelectrodes under inert atmosphere conditions using the following procedure. A 2 μL drop of a benzonitrile/1% pyridine solution containing the alcohol, either ∼40 mM **Fc-BzOH** or ∼10 mM **Por-BzOH**, was first placed on the microelectrode. The organic base pyridine was added to serve two functions:[30,60] (1) to catalyze the reaction of the alcohol with the iodide-terminated surface, and (2) to sponge the HI generated in situ during the displacement of the surface iodine atoms by the alcohol. After addition of the first drop of solution, the Si(100) microelectrode was placed onto a hot plate preheated to either 100 °C (**Fc-BzOH**) or 165 °C (**Por-BzOH**), and the new conditions were maintained as successive 2 μL drops of solution were added to the surface at 20 min intervals up to a total of 3 h. Deposition times longer than 3 h failed to increase the surface coverage, as determined by voltammetric and XPS studies (vide infra). Once the reaction was complete, the Si surfaces were rinsed and sonicated three times with presparged anhydrous CH_2Cl_2 and dried under Ar. The **Fc-BzOH** and **Por-BzOH** monolayers formed on the iodide-modified Si(100) surface using the dropwise-addition procedure at elevated temperatures were found to be superior to those obtained by any of the other methods examined (again, as evaluated by voltammetric studies). This procedure also afforded the highest surface coverage. Additional studies revealed that the surface coverage of the electroactive molecules could be controlled by altering the deposition time and/or by adding an inert species (**BPM**) into the deposition solution for co-attachment.

D. XPS Measurements. XPS was used to characterize both the hydride- and the iodide-modified Si(100) surfaces as well as the surfaces with the **Fc-BzOH** and **Por-BzOH** monolayers. The platforms used for the XPS studies were typically squares 0.25 cm^2 in area. The XPS data were collected using a Leybold EA11-MCD system with a Mg Kα X-ray (1253.6 eV) source. The samples were introduced to the main XPS chamber, which was kept at a base pressure in the 10^{-8} Torr range, by using a fast transferring mechanism consisting of a long rod and an intermediate pumping stage. The total time required for the introduction of the sample was approximately 10 min. In a few control experiments, the Si samples were transported in a sealed holder from the preparation box to the XPS chamber to avoid any exposure to air. However, it was determined that this was not a critical factor once the surfaces were passivated with hydrogen, iodine, or the final alcohols. Spectra were obtained by averaging 10 and 100 scans for the survey and high-resolution runs, respectively. All survey spectra (scans of 1000 eV or more) were taken by using a band-pass energy of 100 eV, which corresponds to a spectral resolution of 2 eV. Additional narrow scans of the main photoelectron lines were obtained with a band-pass energy of 31.5 eV to accurately determine their energy and shape. High-resolution Si 2p, C 1s, and O 1s spectra were taken for all of the surfaces and monolayers, and additional Fe 2p and Zn 2p and N 1s high-resolution data were recorded for the **Fc-BzOH** and **Por-BzOH** monolayers, respectively. To compensate for any charging effects, all of the XPS peak positions were referred to the adventitious hydrocarbon C 1s peak at 284.6 eV.[61]

E. Electrochemical Measurements. All electrochemical measurements were made under inert atmospheres using the setup shown in Figure 2. The section of Si(100) wafer containing the microelectrode was mounted onto a Cu plate using a Ga eutectic to provide good electrical contact through the backside of the wafer. The polypropylene micropipet tip containing the Ag counter/reference electrode and filled with ∼5 μL of the PC/1.0 M Bu_4PF_6 electrolyte solution was positioned over the microvia using a micropositioner. The probe was set so only a small meniscus of the electrolyte protruded from the end of the pipet tip. The end of the pipet tip was then lowered until the surface was wetted by the meniscus of the electrolyte solution (Figure 2, inset). The nature of the junction and the surface tension of the highly viscous PC solution allowed for only a small amount of electrolyte (<1 μL) to spread across the surface. The low volatility of PC precludes any problems that might arise from evaporation of the very small volumes of solvent used in the experiment.

1. Voltammetric Characterization. The **Fc-BzOH** and **Por-BzOH** monolayers were characterized using cyclic voltammetry at scan rates ranging from 1 to 200 V s^{-1}. The potential window ranged from 0 to 1.3 V. The voltammograms were recorded with a Gamry Instruments PC4-FAS1 femtostat running PHE200 Framework and Echem Analyst software. The surface coverage of the redox-active molecules in the monolayers was determined via integration of the voltammetric waves.

2. Determination of Electron-Transfer Rates. The standard electron-transfer rate constants (k^0) of the **Fc-BzOH** and **Por-BzOH** monolayers were measured using a variation of an AC voltammetric technique developed by Creager and co-workers.[62,63] In the method of Creager and co-workers, the AC voltammetric current obtained at the formal DC offset potential (I_{peak}) is ratioed against that obtained at a background potential well below the formal potential (I_{bkgd}). The I_{peak}/I_{bkgd} data are collected for a series of frequencies, and the k^0 values are extracted by fitting the plot to a Randles equivalent circuit model. In our variation of the method of Creager and co-workers, data sets are

(53) Terry, J.; Linford, M. R.; Wigren, C.; Cao, R.; Pianetta, P.; Chidsey, C. E. D. *Appl. Phys. Lett.* **1997**, *71*, 1056−1058.
(54) Waltenburg, H. N.; Yates, J. T., Jr. *Chem. Rev.* **1995**, *95*, 1589−1573.
(55) Cheng, C. C.; Lucas, S. R.; Gutleben, H.; Choyke, W. J.; Yates, J. T., Jr. *J. Am. Chem. Soc.* **1992**, *114*, 1249−1252.
(56) Bergerson, W. F.; Mulder, J. A.; Hsung, R. P.; Zhu, X. Y. *J. Am. Chem. Soc.* **1999**, *121*, 454−455.
(57) Haber, J. A.; Lauermann, I.; Michalak, D.; Vaid, T. P.; Lewis, N. S. *J. Phys. Chem. B* **2000**, *104*, 9947−9950.
(58) Haber, J. A.; Lewis, N. S. *J. Phys. Chem. B* **2002**, *106*, 3639−3656.
(59) Cai, W.; Lin, Z.; Strother, T.; Smith, L. M.; Hamers, R. J. *J. Phys. Chem. B* **2002**, *106*, 2656−2664.
(60) Klaus, J. W.; Sneh, O.; George, S. M. *Science* **1997**, *278*, 1934−1936.
(61) *Handbook of X-ray Photoelectron Spectroscopy*; Wagner, C. D., Riggs, W. M., Davis, L. E., Moulder, J. F., Muilenberg, G. E., Eds.; Perkin-Elmer Corp.: Eden Prairie, 1978.
(62) Li, J.; Schuler, K.; Creager, S. E. *J. Electrochem. Soc.* **2000**, *147*, 4584−4588.
(63) Creager, S. E.; Wooster, T. T. *Anal. Chem.* **1998**, *70*, 4257−4263.

not obtained at discrete frequencies, but rather the frequency of the sinusoidal potential waveform is swept in time.[17] The data generated in the swept waveform voltammetric (SWAV) experiment are then Fourier transformed to obtain a conventional current-frequency plot. The details of the SWAV experiment and its use to measure the electron-transfer kinetics of thiol-derivatized porphyrin monolayers on Au surfaces are described in our previous report of the experiments on Au surfaces.[17]

3. Determination of Charge-Retention Times. The charge-retention characteristics of the **Fc-BzOH** and **Por-BzOH** monolayers were determined using open circuit potential amperometry (OCPA). The details of the OCPA experiment and its use to measure charge retention in thiol-derivatized porphyrin monolayers on Au surfaces have been described in a number of earlier publications.[7−10] The reader is referred to ref 10 for a full description of the temporal behavior of background versus faradaic currents and the stability of the OCP. In brief, the OCPA experiment is performed as follows. Initially, the monolayer is oxidized with a 20 ms pulse ~100 mV above the formal potential of the desired redox state. The pulse time was chosen to be much longer than the RC constant of the cell to avoid any interference from the cell response with our measurements. Next, the applied potential is disconnected from the counter/reference electrode for a variable period of time to probe the kinetics of charge dissipation in the absence of an applied field. During the disconnect time, the electrochemical cell relaxes to the open circuit potential (OCP), after which the applied potential is changed to match the empirically determined OCP. The counter electrode is then reconnected, and the resulting current is monitored as the monolayer is reduced (because the OCP is at a reducing potential). The magnitude of the observed current is directly proportional to the number of molecules that remain oxidized on the surface while the counter electrode is disconnected. Charge retention is measured by successively changing the disconnect time up to a point where essentially all of the molecules that were initially oxidized decay back to the neutral state. In previous studies of thiol-derivatized porphyrin monolayers on Au, we have found that the charge-dissipation process follows approximately first-order kinetics;[7−10] accordingly, we have found it convenient to characterize charge retention in terms of a half-life ($t_{1/2}$). Similar behavior is found for the monolayers on Si(100) studied herein.

III. Results

A. Si(100) Surface Characteristics and Their Relationship to Monolayer Formation. The Si(100) surface was examined by XPS after each step of the chemical modification process. These experiments were performed to determine the optimum surface characteristics for monolayer formation and to aid in determining why certain surfaces yielded poor quality monolayers. Extensive studies of both the hydride- and the iodide-modified surfaces revealed that surface oxidation was the most likely factor in compromising the formation of good quality monolayers. This observation prompted us to perform all experiments under inert atmosphere conditions and to vigorously remove any physisorbed water from the surfaces. Under these conditions, hydride-passivated surfaces free from any noticeable surface oxidation were readily obtained. Specifically, only one Si 2p XPS peak was seen at 98.5 eV; the wide Si 2p shoulder band at 103.3 eV indicative of SiO_2 was absent. The extent of carbon contamination was also minimal under these conditions. Iodide modification of the surface was detected by the appearance of new XPS bands at 618.8 and 630.5 eV, corresponding to I $3d_{5/2}$ and I $3d_{3/2}$, respectively, as well as a strong core I Auger line at 736.4 eV and weaker I $3p_{3/2}$ and I $3p_{1/2}$ lines at 874.1 and 930.1 eV, respectively. The sharp and symmetric shapes of the I 3d XPS peaks in the high-resolution spectra suggest a monodisperse Si−I derivatized surface.[58] On the other hand, the Si(100) surface was found to be particularly prone to oxidation during the iodide modification process. This was evidenced by the appearance of an O 1s line at 532.1 eV, along with a positive shift in the Si 2p line to a higher binding energy, about 99.4 eV. The high binding energy of the O 1s XPS peak is more in line with hydroxide surface moieties, suggesting that the oxidation of the surface is induced by water, not O_2.[64] Performing the iodine derivatization step under inert atmosphere conditions for the most part eliminated the surface oxidation.

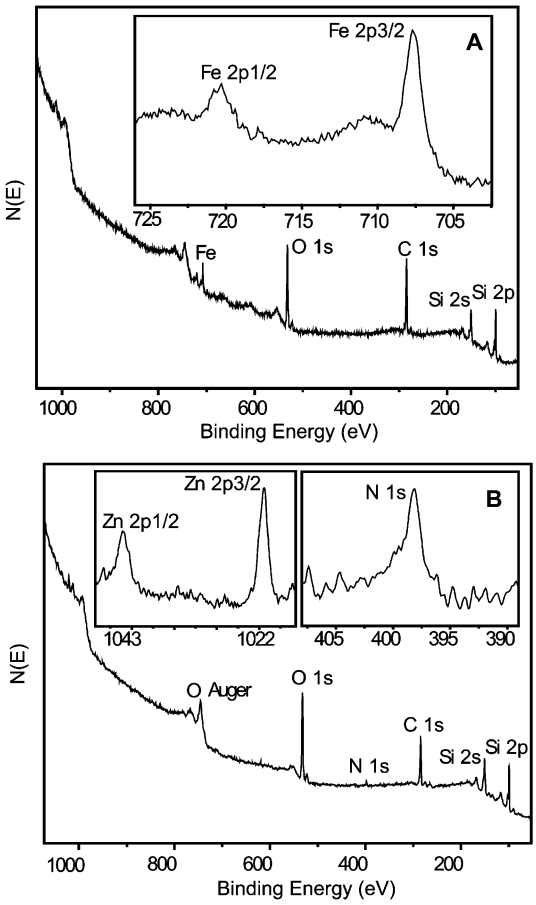

Figure 3. XPS of the (A) **Fc-BzOH** and (B) **Por-BzOH** monolayers on bulk *p*-type Si(100) substrates. Insets: Expanded regions showing the bands due to (A) Fe and (B) Zn and N.

Representative XPS spectra of the **Fc-BzOH** saturated monolayers are shown in Figure 3A. In addition to the bands due to Si, signals are observed for Fe, O, and C as well. The Fe $2p_{3/2}$ and Fe $2p_{1/2}$ peaks, clearly visible at 707.8 and 720.4 eV, respectively, in the high-resolution spectrum shown in the inset, are consistent with values reported in the literature.[65−67] Close inspection of the main survey spectrum also reveals the weak Fe Auger lines at about 550, 600, and 655 eV. By calibration of the different XPS peak intensities using reported sensitivity factors,[61] a coverage on the order of 1.5×10^{-10} mol cm^{-2} is estimated for **Fc-BzOH**, somewhat lower than the values obtained by voltammetry (vide infra). However, the concentra-

(64) Barr, T. L. *J. Phys. Chem.* **1978**, *82*, 1801−1810.
(65) Woodbridge, C. M.; Pugmire, D. L.; Johnson, R. C.; Boag, N. M.; Langell, M. A. *J. Phys. Chem. B* **2000**, *104*, 3085−3093.
(66) Gassman, P. G.; Macomber, D. W.; Hershberger, J. W. *Organometallics* **1983**, *2*, 1470−1472.
(67) Cowan, D. O.; Park, J.; Barber, M.; Swift, P. *J. Chem. Soc. D* **1971**, 1444−1446.

tion determined from the XPS data requires certain assumptions regarding the thickness of the monolayers and is therefore not accurate to better than a factor of 2. In any case, the absence of any I 3d XPS signal following the attachment of **Fc-BzOH** indicates that the exchange of surface-terminated iodide atoms is quantitative. On the other hand, even though the **Fc-BzOH** monolayer contributes to the bands at 284.6 and 532.1 eV due to C 1s and O 1s, respectively, a quantitative analysis indicates that at least one-half of the carbon and almost 90% of the oxygen signals in the XPS data originate from other surface species. The development of adventitious surface oxide during the derivatization process is also evidenced by the reappearance of a shoulder at 103.3 eV on the main Si 2p band. Surface oxidation was found to occur even under the inert conditions used for the attachment of the monolayer, leading us to speculate that, again, the oxidation is most likely due to the presence of trace amounts of residual water in the anhydrous solvents used for the deposition. The elevated temperature used for the deposition process may further promote surface oxidation.

Representative XPS spectra of the **Por-BzOH** saturated monolayers are shown in Figure 3B. The spectral changes elicited by attachment of this compound to the Si(100) surface are generally similar to those described above for the **Fc-BzOH** monolayers. In particular, new XPS bands due to atoms in the attached monolayer (Zn, N, C, and O) are observed, and no signal associated with I is seen, indicating quantitative exchange of the surface iodide. The Zn $2p_{3/2}$ and Zn $2p_{1/2}$ peaks are identified at 1019.7 and 1042.6 eV, respectively (high-resolution spectrum in Figure 3B, inset), and a band due to the N 1s from the N atoms in the porphyrin ring is visible at 398.3 eV. The binding energies measured here for the Zn 2p photoelectrons are somewhat lower than those reported for similar porphyrins in the past (Zn $2p_{3/2} \approx 1021.5$ eV),[68] but the value for the N 1s agrees quite well with previous studies.[68,69] The surface coverage of the porphyrin is estimated from the XPS data to be about 5 times lower than that in the case of the ferrocene. Unlike the absolute value of the surface coverage, the estimates of the relative surface concentrations between the two electroactive molecules should be more reliable. Also, the N 1s XPS intensity can be fully accounted for by the presence of the adsorbed **Por-BzOH** (a 4:1 N:Zn atomic ratio), but, again, one-half of the C 1s and almost all of the O 1s peaks correspond to other surface species that are formed during deposition of the **Por-BzOH** monolayers.

B. Voltammetric Characteristics of the Monolayers. Representative fast-scan cyclic voltammograms for the **Fc-BzOH** and **Por-BzOH** monolayers are shown in Figure 4 (panels A and B, respectively). The two waves observed for **Por-BzOH** correspond to the mono- and dication radicals. The traces reported in this figure correspond to surface concentrations of 4.2×10^{-10} and 6.4×10^{-11} mol cm^{-2} for **Fc-BzOH** and **Por-BzOH**, respectively, and to 10, 25, 50, 75, and 100 V s^{-1} scan rates, from the smallest to the largest amplitude. Both the general appearance of the voltammograms of the monolayers of both molecules and the $E_{1/2}$ values are very similar to those observed for the analogous thiol-derivatized molecules (designated **Fc-BzSH** and **Por-BzSH**, respectively) self-assembled onto Au(111) surfaces (Roth, K.; Kuhr, W. G.; Bocian, D. F., unpublished).[7,17]

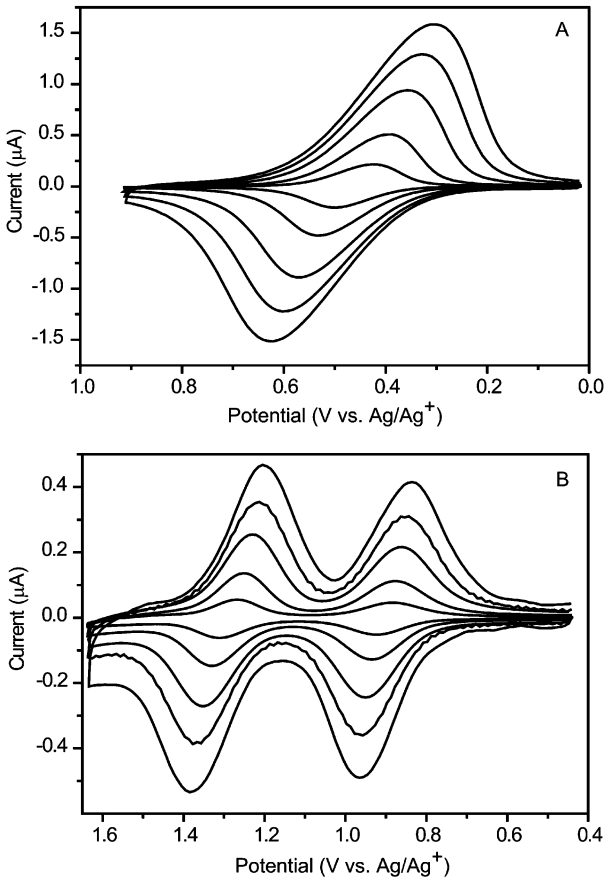

Figure 4. Representative fast-scan cyclic voltammograms of the monolayers on *p*-type Si(100) microelectrodes in PC/1.0 M Bu_4NPF_6. (A) **Fc-BzOH** monolayer: $\Gamma \approx 4.2 \times 10^{-10}$ mol cm^{-2}; $E_{1/2} \approx 0.48$ V. (B) **Por-BzOH** monolayer: $\Gamma \approx 6.4 \times 10^{-11}$ mol cm^{-2}; $E_{1/2}{}^{0/+1} \approx 0.90$ V; $E_{1/2}{}^{+1/+2} \approx 1.30$ V. The scan rates are 10, 25, 50, 75, and 100 V s^{-1} from smallest to largest amplitude.

Both the **Fc-BzOH** and the **Por-BzOH** monolayers exhibit robust, reversible voltammetric behavior. Under inert atmosphere conditions, the voltammetric characteristics of the **Fc-BzOH** and **Por-BzOH** monolayers are stable over repeated cycling through a large number of scans ($\sim 10^8$, conducted over a period of days). The stability of neat monolayers, that is, without co-attached **BPM**, was markedly better at high coverages than at lower coverages, presumably because of blockage of access to the surface by trace water (or other materials) that could initiate surface deterioration. Consistent with this notion, the use of **BPM** as a co-attached species on surfaces where the coverage of electroactive molecules was low rendered the monolayers much more stable. Therefore, **BPM** was used in all studies where the surface concentration was varied (vide infra). Under ambient conditions, the monolayers were generally less stable whether **BPM** was present or not, showing noticeable degradation after a few thousand cycles, or even in the absence of cycling after a few hours.

There are several other noteworthy features of the voltammetric behavior of the **Fc-BzOH** and **Por-BzOH** monolayers, many of which parallel those observed for the **Fc-BzSH** and **Por-BzSH** SAMs on Au(111) surfaces,[7,17] as well as for related molecules on Au(111).[8−14,16]

(68) Polzonetti, G.; Ferri, A.; Russo, M. V.; Iucci, G.; Licoccia, S.; Paolesse, R. *J. Vac. Sci. Technol., A* **1999**, *17*, 832−839.
(69) Zhang, Z.; Hu, R.; Liu, Z. *Langmuir* **2000**, *16*, 1158−1162.

(1) The voltammetric behavior of the **Fc-BzOH** and **Por-BzOH** monolayers on Si(100) at low surface coverage is not affected by the presence of the co-attached **BPM**. This result suggests that the molecules do not cluster on the surface upon deposition. Clustering would give rise to strong electrical interactions, at least in the case of the **Fc-BzOH** monolayers where the redox centers are not screened from one another by the presence of bulky substituent groups. A less pronounced effect would be expected for the **Por-BzOH** monolayers, because the bulky mesityl groups impart significant self-screening to the porphyrin cations.[17]

(2) The half-wave potentials ($E_{1/2}$) for both the **Fc-BzOH** and the **Por-BzOH** monolayers on Si(100) are more positive than those observed for the same molecules in solution. Moreover, the magnitude of the positive potential shift for the monolayer depends on the surface coverage (Γ). For example, while the potential for **Fc-BzOH** in solution is $E_{1/2} \approx 0.20$ V, it exhibits a value of $E_{1/2} \approx 0.33$ V when attached to Si(100) at relatively low surface coverages ($\Gamma \approx 1.9 \times 10^{-12}$ mol cm^{-2}) and reaches $E_{1/2} \approx 0.47$ V at $\Gamma \approx 5.4 \times 10^{-11}$ mol cm^{-2}. For **Por-BzOH**, the potentials are ${E_{1/2}}^{0/+1} \approx 0.64$ V and ${E_{1/2}}^{+1/+2} \approx 0.90$ V in solution, ${E_{1/2}}^{0/+1} \approx 0.72$ V and ${E_{1/2}}^{+1/+2} \approx 1.0$ V for $\Gamma \approx 2.0 \times 10^{-12}$ mol cm^{-2} on the surface, and ${E_{1/2}}^{0/+1} \approx 0.83$ V and ${E_{1/2}}^{+1/+2} \approx 1.2$ V for $\Gamma \approx 1.1 \times 10^{-11}$ mol cm^{-2}. These trends continue as the surface coverage increases further: for both the **Fc-BzOH** and the **Por-BzOH** monolayers, the maximum potential shift relative to that observed in solution is ~0.25 V.

(3) The anodic and cathodic peak maxima (ΔE_{pp}) for both the **Fc-BzOH** and the **Por-BzOH** monolayers on Si(100) are split. The value of ΔE_{pp} at a given scan rate varies with surface coverage, as does the full-width at half-maximum of the peak (E_{fwhm}). In the examples that follow, the scan rate is 100 V s^{-1}. For the **Fc-BzOH** monolayer at low surface coverage ($\Gamma \approx 1.9 \times 10^{-12}$ mol cm^{-2}), $\Delta E_{pp} \approx 35$ mV and $E_{fwhm} \approx 130$ mV. At higher surface coverage ($\Gamma \approx 5.4 \times 10^{-11}$ mol cm^{-2}), $\Delta E_{pp} \approx 51$ mV and $E_{fwhm} \approx 140$ mV. For **Por-BzOH** at low surface coverage ($\Gamma \approx 2.0 \times 10^{-12}$ mol cm^{-2}), $\Delta E_{pp} \approx 65$ mV and $E_{fwhm} \approx 130$ mV. At higher surface coverage ($\Gamma \approx 1.1 \times 10^{-11}$ mol cm^{-2}), $\Delta E_{pp} \approx 84$ mV and $E_{fwhm} \approx 160$ mV. The surface-coverage dependence of ΔE_{pp} and ΔE_{fwhm} could reflect either kinetic or thermodynamic effects (or both). However, we note that our measurements were conducted with a two-electrode cell. In the two-electrode configuration, the effects of IR drop, which would become more important as the surface coverage increases (due to the higher currents), can potentially complicate the determination of redox kinetics from the voltammetric behavior using traditional Nicholson−Shain methodology. Therefore, all kinetic measurements were made using the SWAV technique.

(4) The voltammetric characteristics of the **Fc-BzOH** and **Por-BzOH** monolayers on the *p*-type Si(100) surface exhibit no noticeable sensitivity to illumination. This result shows that electron transfer is not limited by the number of carriers in the semiconductor, a behavior expected because the redox potentials of the monolayers, which are +500 mV or greater, are well above the flat-band potential of the *p*-type Si(100), which is in the range from 0 to −100 mV.[46] Applied potentials of +500 mV (or greater) will shift the Fermi level well into the valence band of the heavily dope *p*-type Si.

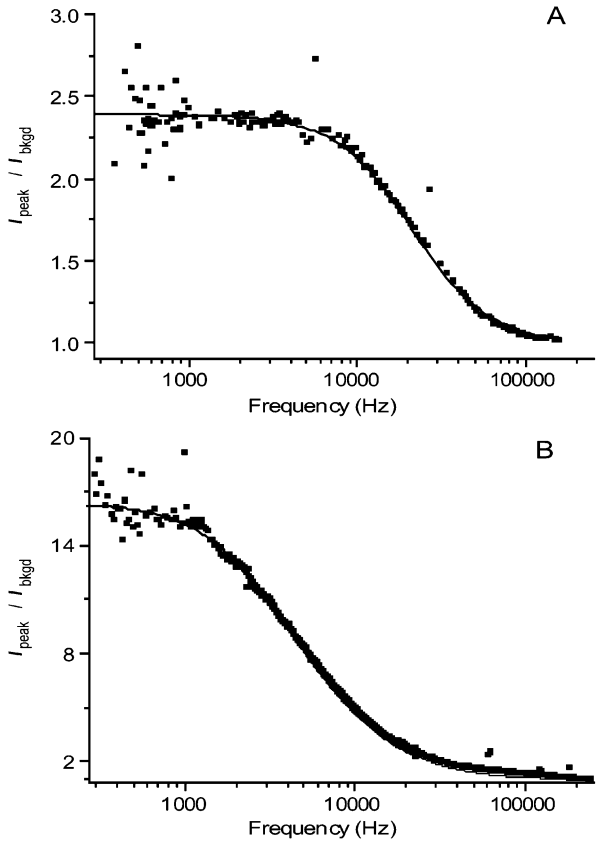

Figure 5. I_{peak}/I_{bkgd} (■) versus frequency for the (A) **Fc-BzOH** and (B) **Por-BzOH** monolayers. The solid lines represent fits to the data using a Randles equivalent circuit. The fitting parameters are as follows: (A) **Fc-BzOH** monolayer: $k^0 \approx 4.5 \times 10^4$ s^{-1}; $\Gamma \approx 1.3 \times 10^{-12}$ mol cm^{-2}. (B) **Por-BzOH** monolayer: $k^0 \approx 0.90 \times 10^4$ s^{-1}; $\Gamma \approx 2.0 \times 10^{-11}$ mol cm^{-2}. **BPM** served as the co-attached species for both monolayers.

C. Electron-Transfer Characteristics of the Monolayers. Representative plots of I_{peak}/I_{bkgd} for the **Fc-BzOH** and **Por-BzOH** monolayers are shown in Figure 5 (panels A and B, respectively). The data for I_{peak} were taken at the measured $E_{1/2}$; the data for I_{bkgd} were taken at an *E*-value 150 mV negative of the $E_{1/2}$. In the case of the **Por-BzOH** monolayers, the electron-transfer kinetics were examined only for the monocation. Electron-transfer rate constants of $k^0 \approx 4.5 \times 10^4$ and 0.90×10^4 s^{-1} (±10%) were obtained for the **Fc-BzOH** and **Por-BzOH** monolayers, respectively, by fitting the data shown in Figure 5.

Clearly, the k^0 values for the **Fc-BzOH** versus **Por-BzOH** monolayers are quite different. However, as examined below, this is not due to a large intrinsic difference in electron-transfer behavior between the two types of monolayers, but rather to differences in surface coverage. The data shown for the **Fc-BzOH** monolayer were obtained for a relatively low surface coverage of redox-active molecules ($\Gamma \approx 1.3 \times 10^{-12}$ mol cm^{-2}), whereas the data shown for the **Por-BzOH** monolayer were obtained at much higher surface concentration ($\Gamma \approx 2.0 \times 10^{-11}$ mol cm^{-2}). The higher surface coverage of the **Por-BzOH** monolayer is reflected in the much larger I_{peak} values measured at low frequencies.

The coverage dependence of the electron-transfer rates was studied in more detail. The k^0 values obtained for the **Fc-BzOH** and **Por-BzOH** monolayers at surface coverages ranging from

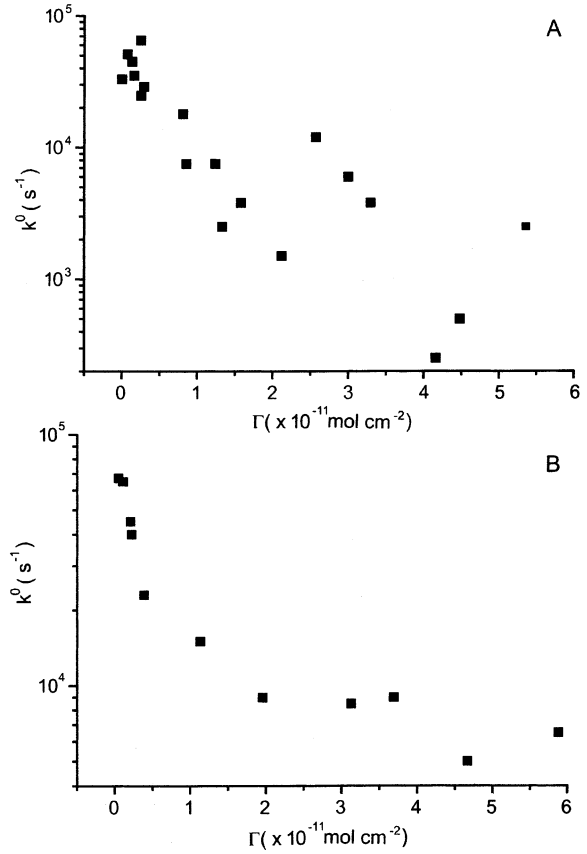

Figure 6. Plot of k^0 values versus Γ for the (A) **Fc-BzOH** and (B) **Por-BzOH** monolayers. **BPM** served as the co-attached species for all experiments.

$\Gamma \approx 10^{-12}$ mol cm^{-2} to $\Gamma \approx 6 \times 10^{-11}$ mol cm^{-2} are plotted in semilogarithmic fashion in Figure 6.

The qualitative behavior observed for both types of monolayers is similar, although the absolute rate values at any given surface coverage are quite different for the two systems. In particular, at a very low surface concentration ($\Gamma \approx 10^{-12}$ mol cm^{-2}), electron transfer is relatively fast ($k^0 > 5 \times 10^4$ s^{-1}), but as the surface concentration is increased into the $\Gamma \approx 10^{-11}$ mol cm^{-2} range, the rates fall steeply, and above $\Gamma \approx 2 \times 10^{-11}$ mol cm^{-2}, they level off. The limiting electron-transfer rate values for the **Fc-BzOH** and **Por-BzOH** monolayers are $k^0 \approx 10^3$ and $k^0 \approx 5 \times 10^3$ s^{-1}, respectively.

The electron-transfer kinetics of the **Fc-BzOH** and **Por-BzOH** monolayers were also examined at higher surface concentrations than those shown in Figure 6, up to $\Gamma \approx 4 \times 10^{-10}$ mol cm^{-2} for **Fc-BzOH** and $\Gamma \approx 1 \times 10^{-10}$ mol cm^{-2} for **Por-BzOH**. However, at coverages above $\Gamma \approx 6 \times 10^{-11}$ mol cm^{-2}, the fits to the plots I_{peak}/I_{bkgd} versus frequency were poor, as was also observed in our previous studies of thiol-derivatized porphyrins assembled on Au.[17] We have attributed this degradation in the fits with increasing surface coverages to an increase in heterogeneity in the monolayer of the redox-active species.

D. Charge-Retention Characteristics of the Monolayers. The charge-retention characteristics of the **Fc-BzOH** and **Por-BzOH** monolayers were examined in parallel with the redox kinetics. Representative data sets for the two monolayers are shown in Figure 7. Panels A and C show the reductive currents measured from the oxidized **Fc-BzOH** and **Por-BzOH** monolayers, respectively, after selected disconnect times followed by reconnection at the OCP (wherein the molecules that have remained oxidized are reduced), and panels B and D show the corresponding charge densities obtained by integration of those current transients. The charge-retention measurements shown are for the same monolayers used for the electron-transfer studies in Figure 5. The $t_{1/2}$ values obtained for **Fc-BzOH** and **Por-BzOH** by fitting these and additional data for a number of disconnect times were ∼20 and ∼150 s, respectively. As in the case for the electron-transfer rates, the differences in charge-retention times do not reflect intrinsic differences between the behavior of the two types of monolayers, but rather differences in surface coverages (vide infra). In particular, the **Fc-BzOH** monolayer, which corresponds to a relatively low surface coverage ($\Gamma \approx 1.3 \times 10^{-12}$ mol cm^{-2}), exhibits much faster loss of charge (shorter $t_{1/2}$) than the higher coverage ($\Gamma \approx 2.0 \times 10^{-11}$ mol cm^{-2}) **Por-BzOH** monolayer. The kinetics of charge dissipation (no applied potential) parallel the kinetics of electron transfer (presence of applied potential). In particular, monolayers at low coverage exhibit generally faster kinetics for both processes than do monolayers at high coverage.

The $t_{1/2}$ values obtained for the **Fc-BzOH** and **Por-BzOH** monolayers at surface coverages ranging from $\Gamma \approx 10^{-12}$ mol cm^{-2} to $\Gamma \approx 6 \times 10^{-11}$ mol cm^{-2} are plotted in Figure 8 (panels A and B, respectively). Again, these $t_{1/2}$ values and the k^0 values at a given concentration (Figure 6) were obtained on the same monolayers. Inspection of Figure 8 reveals that the charge-dissipation behavior for the two types of monolayers is qualitatively similar (as is the case for the electron-transfer kinetics). At very low surface concentration ($\Gamma \approx 10^{-12}$ mol cm^{-2}), relatively rapid charge dissipation occurs ($t_{1/2} < 20$ s), but as the surface concentration is increased, the rates fall relatively steeply, and above $\Gamma \approx 2 \times 10^{-11}$ mol cm^{-2}, they level off to half-life times in the $t_{1/2} \approx 150-200$ s range. The similarity in the trends observed for the charge-dissipation and electron-transfer kinetics as a function of surface concentration is perhaps even closer than suggested by the data in Figure 8 because of the variations in the measured $t_{1/2}$ value for a given monolayer, typically ±20% at high surface coverages, and even larger at a low surface coverage (where the charge-retention times are relatively short).

IV. Discussion

The studies reported herein both establish a relatively general protocol for attaching redox-active molecules to Si surfaces and provide a foundation for understanding the electron-transfer rates and charge-retention properties of the resulting monolayers. The first theme that emerges from these studies is that the method of attaching the molecules to the Si substrate is key for obtaining robust monolayers on which reliable measurements can be made. A second identifiable theme is that the redox-kinetic and charge-retention characteristics of the **Fc-BzOH** and **Por-BzOH** monolayers on Si are generally similar to one another. These similarities include both the absolute magnitudes of the electron-transfer and charge-dissipation rates and the trends observed in these rates as a function of the surface coverage of the molecules. A third theme is that the redox-kinetic and charge-retention characteristics of the **Fc-BzOH** and **Por-BzOH** monolayers on Si exhibit a number of features in common with

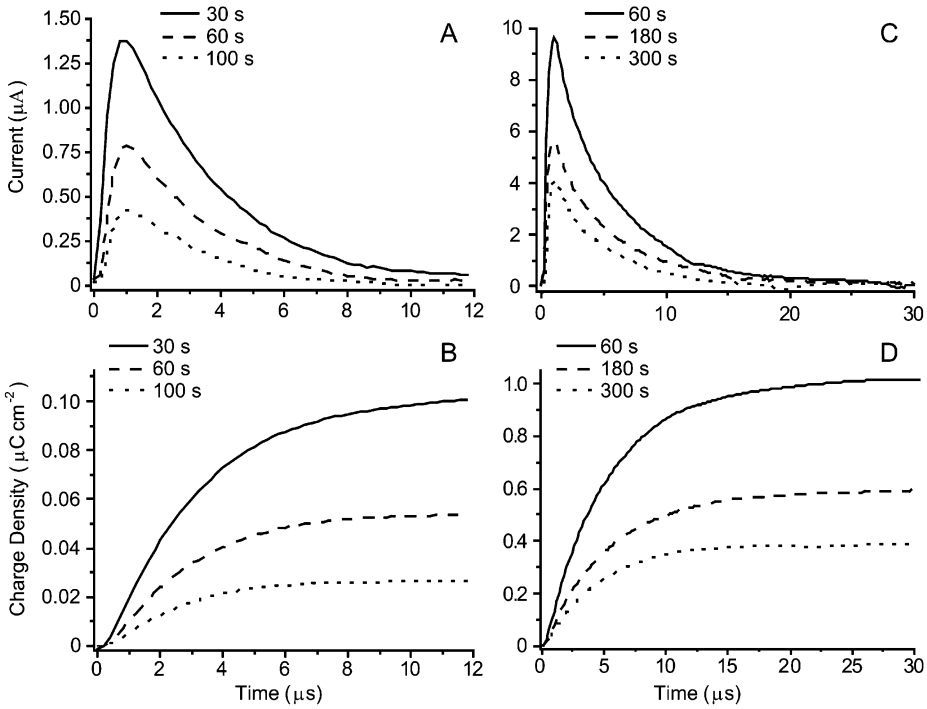

Figure 7. Reductive current transients observed from the oxidized monolayers after selected disconnect times and reconnection at the OCP. (A) **Fc-BzOH**: Oxidized at 450 mV; reconnected at the measured OCP of 100 mV. (C) **Por-BzOH**: Oxidized at 900 mV; reconnected at the measured OCP of 150 mV. Charge density in the (B) **Fc-BzOH** and (D) **Por-BzOH** monolayers obtained by integrating the current transients in A and C, respectively. The charge-retention measurements shown are for the same monolayers whose electron-transfer characteristics are shown in Figure 5. The $t_{1/2}$ values, determined via analysis of the complete set of current transients for the **Fc-BzOH** and **Por-BzOH** monolayers, were determined to be ∼20 and ∼150 s, respectively.

those of thiol-derivatized molecules tethered to Au surfaces. However, there are also certain clear differences between the behavior of **Fc-BzOH** versus **Por-BzOH** on Si(100) as compared with **Fc-BzSH** versus **Por-BzSH** on Au(111) surfaces. In the sections below, we discuss these three themes in more detail.

A. Effect of Attachment Process on Monolayer Characteristics. The importance of the development of a molecular attachment process that yields stable and relatively homogeneous monolayers cannot be overemphasized. The implementation of previously reported methods either failed to yield any molecular attachment or led to poor quality monolayers highly susceptible to damage during the course of the electrochemical measurements, as evidenced by loss of electrochemical response over time. The surfaces for which the quality of the monolayers was poor were also quite susceptible to oxidative damage during the electrochemical measurements, even under inert atmosphere conditions. It should also be noted that, due to steric effects, not all Si sites on the surface can be derivatized with the electroactive molecules of interest, in particular when bulky porphyrins are used. This leaves a large fraction of Si atoms susceptible to attack by degradative agents such as water. One successful strategy to minimize this effect is the use of inert co-attached species, such as **BPM** in our studies. The capping of the final architecture with a viscous electrolyte for device manufacturing also aids in the protection of the redox-modified Si layers.

It is also important to note that previous strategies for attaching alcohol-derivatized molecules to Si utilized neat liquids or highly soluble (in the deposition solvent) molecules. In such cases, the concentration of the molecules is extremely high, and kinetic effects do not limit the reaction with the Si surface. These

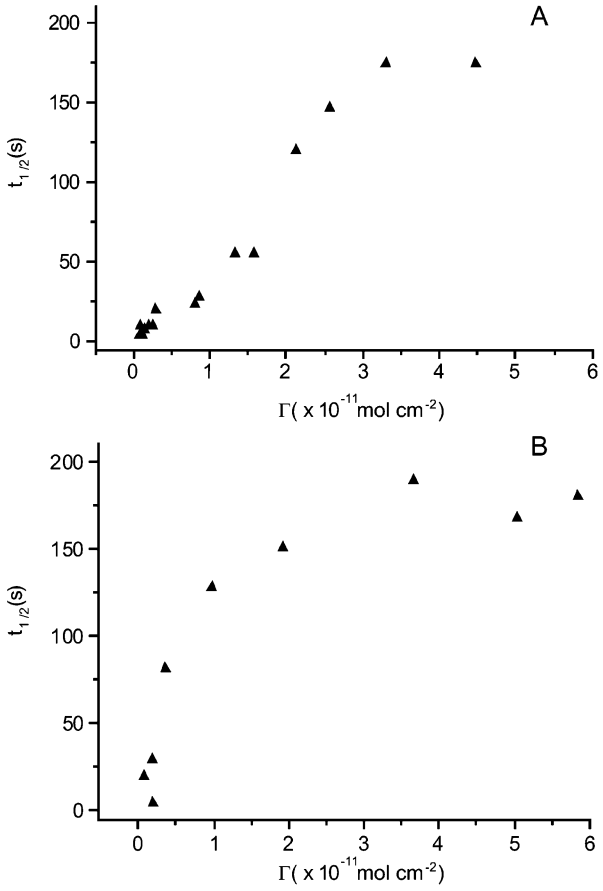

Figure 8. Plot of $t_{1/2}$ values versus Γ for the (A) **Fc-BzOH** and (B) **Por-BzOH** monolayers. Each $t_{1/2}$ value was obtained from the same monolayer as that used to determine the k^0 at a particular surface coverage (Figure 6).

attachment methods fail completely for molecules at low concentrations. In contrast, our attachment strategy provides access to high-quality monolayers over a large range of surface coverage even for molecules with limited solubility in the deposition solution. This issue is less important for **Fc-BzOH**, which is highly soluble in solvents suitable for deposition, but is paramount for **Por-BzOH** and other types of porphyrin-containing compounds, whose solubility is generally <100 mM and often <10 mM. Our attachment protocol also affords good control of the surface concentration of the electroactive molecules, thus yielding monolayers with highly reproducible surface coverage.

B. Electrochemical Characteristics of the Fc-BzOH and Por-BzOH Monolayers on Si(100). The relatively high dopant levels ($\sim 10^{18}$ cm^{-3}) of the *p*-type Si(100) substrate used in these studies, together with the relatively positive redox potentials for formation of the **Fc-BzOH** and **Por-BzOH** cations, ensure that the electrochemical measurements performed on the monolayers reflect their intrinsic characteristics rather than limiting electrical properties of the Si surface. In particular, the measurements were not limited by space-charge effects in the semiconductor because the Si electrode was operating in carrier accumulation mode.[46] Under those conditions, holes accumulate at the surface of the electrode, and a behavior similar to that of an inert metal is observed.[44] The reversible voltammetric response exhibited by both the **Fc-BzOH** and the **Por-BzOH** monolayers and the insensitivity of the voltammetric characteristics to illumination attest to the good electrical response of our electrodes.

Our studies revealed that the electron-transfer and charge-dissipation kinetics of the **Fc-BzOH** and **Por-BzOH** monolayers on Si(100) are generally similar to one another and follow similar trends as a function of surface coverage. This observation seems inherently reasonable because both molecules have the same benzyloxy tether to the Si surface. The suggestion is that the electron-transfer behavior of these monolayers is controlled by the nature and characteristics of the linking group. The fact that the Si−O bond is strong may also be a determining factor for orientation of the redox-active molecules on the surface. This is not necessarily the case for a weaker bond such as Au−S, as will be discussed in more detail below.

The behavior discussed above is further complicated by the fact that the electron-transfer and charge-dissipation rates for both the **Fc-BzOH** and the **Por-BzOH** monolayers on Si(100) are affected by surface concentration, exhibiting a monotonic decrease in rate with increasing surface concentration. In fact, similar trends were previously reported for thiol-derivatized porphyrin SAMs on Au surfaces.[17] This behavior has been attributed to the formation of a space-charge region caused by an extended layer of counterions, in this case anions, migrating toward the oxidized monolayer to balance the positive charge. Such an effect may be exacerbated in a tightly packed monolayer, which hinders access of the counterions/solvent. As the surface coverage increases, the space-charge and counterions/solvent exclusion effects may slow the electron-transfer and charge-dissipation rates and also shift the formal potential to more positive values. Accordingly, this explanation predicts that monolayer packing exerts both kinetic (slowing of electron-transfer and charge-dissipation rates) and thermodynamic effects (formal potential shifts).[17] At high surface coverage, limiting slow rates are reached for both electron transfer and charge dissipation. These rates do not reflect the intrinsic electronic coupling of the redox center to the surface atoms via the linker, but rather bulk properties of the monolayer-counterion/solvent milieu. The intrinsic electron-transfer and charge-dissipation rates are reflected in the k^0 and $t_{1/2}$ values observed at low surface coverage (e.g., $\Gamma \leq 1 \times 10^{-12}$ mol cm^{-2}). These values are $k^0 \approx 6.5 \times 10^4$ s^{-1} and $t_{1/2} \approx 10$ s for both monolayers.

Alternatively, the changes in electron-transfer and charge-retention rates with surface coverage may reflect differences in the molecular environment at different surface coverages. These differences would necessarily have to occur despite the fact that the total surface coverage of electroactive molecules plus the inert co-attached **BPM** molecules is approximately constant in all of the experiments. For example, if the orientation of the redox-active molecules changes as a function of their surface concentration, the distance between the redox center and the surface changes. If electronic interactions can occur directly between the redox center and the surface (as opposed to (or in addition to) through the relatively short linker), changes in orientation would alter these interactions. It has previously been argued that, by acting as tunneling barriers, inert monolayers may render electron transfer the rate-limiting process in the flow of current across interfaces.[40,41,70] Studies varying the thickness of those monolayers have revealed an exponential dependence of the rate on tunneling distance.[41,44] In this connection, the variation in electron-transfer and charge-dissipation rates at the lowest surface coverages shown in Figures 6 and 8 follows the approximately exponential behavior with coverage seen for other surface phenomena such as adsorption[71−73] and chemical reactions.[74] This type of rate change with coverage has often been associated with changes in activation energies induced by interactions among molecules as they become more tightly packed on the surface. An interaction energy among adsorbates on the surface of about 40 kcal per monolayer can be estimated by Arrhenius analysis of the data in Figures 6 and 8, a value within the range of what has been reported for other systems.[75] In many cases, these interadsorbate interactions lead to changes in adsorption geometry.[71,76] Of particular interest here is the reorientation that takes place with increasing coverage reported for short alkyls[77] and alkoxides[78] adsorbed on metal surfaces, from flat-lying at low coverages to close to perpendicular to the surface at saturation. In fact, in those examples, the change in adsorption geometry is not gradual, but rather abrupt once a critical surface coverage is reached, a behavior more in line with what is seen in Figure 6 for the case of **Por-BzOH**. Perhaps at low coverage, the linking groups are oriented flat on the surface, so the redox centers sit close to the surface, hence the fast electron-transfer rates. After reaching coverages on the order of 5×10^{-12} mol cm^{-2}, however, the hydrocarbon linking chains may reorient into a more vertical position, rendering the redox

(70) Weber, K.; Hockett, L.; Creager, S. *J. Phys. Chem. B* **1997**, *101*, 8286−8291.
(71) Zaera, F. *Prog. Surf. Sci.* **2001**, *69*, 1−98.
(72) Wartnaby, C. E.; Stuck, A.; Yeo, Y. Y.; King, D. A. *J. Phys. Chem.* **1996**, *100*, 12483−12488.
(73) Wu, K. J.; Kevan, S. D. *J. Chem. Phys.* **1991**, *95*, 5355−5363.
(74) Zaera, F. *Acc. Chem. Res.* **2002**, *35*, 129−136.
(75) Conrad, H.; Ertl, G.; Koch, J.; Latta, E. E. *Surf. Sci.* **1974**, *43*, 462−450.
(76) Netzer, F. P.; Ramsey, M. G. *Crit. Rev. Solid State Mater. Sci.* **1992**, *17*, 397−475.
(77) Zaera, F.; Hoffmann, H.; Griffiths, P. R. *J. Electron Spectrosc. Relat. Phenom.* **1990**, *54*−*55*, 705−715.
(78) Street, S. C.; Gellman, A. J. *J. Chem. Phys.* **1996**, *105*, 7158−7170.

center farther away from the surface and consequently reducing the tunneling probability of electrons from those moieties to the surface. Therefore, according to this model, it is the adsorption geometry, which is controlled by the surface coverage, and not the nature of the surface or the linking group itself that determines the electron-transfer and charge-retention rates.

C. Electrochemical Characteristics of the Fc-BzOH and Por-BzOH Monolayers on Si(100) versus Fc-BzSH and Por-BzSH SAMs on Au(111). As was previously noted, the behavior of the electrochemical, redox-kinetic, and charge-retention characteristics of the **Fc-BzOH** and **Por-BzOH** monolayers on Si(100) exhibits many features in common with those observed previously for **Fc-BzSH** and **Por-BzSH** SAMs on Au(111).[10,17] Nevertheless, there are certain notable differences:

(1) The intrinsic (low surface coverage) electron-transfer rate for the **Fc-BzOH** monolayers on Si(100) ($k^0 \approx 6.5 \times 10^4$ s^{-1}) is appreciably slower than that for the **Fc-BzSH** SAMs on Au(111) ($k^0 > 30 \times 10^4$ s^{-1}). The electron-transfer rate for the **Por-BzOH** monolayers on Si(100) is also slower ($k^0 \approx 6.5 \times 10^4$ s^{-1}) than that for **Por-BzSH** on Au(111) ($k^0 \approx 10 \times 10^4$ s^{-1}). However, the difference is not as large as that for the ferrocenes on the two types of surfaces.

(2) The trends observed in the charge-dissipation rates for the monolayers parallel the trends observed for the electron-transfer kinetics. In particular, the charge-retention times for the **Fc-BzOH** monolayer on Si(100) at low surface coverages are much longer ($t_{1/2} \approx 10$ s) than those observed for the **Fc-BzSH** SAM on Au(111) ($t_{1/2} < 1$ s). On the other hand, the charge-retention times for the **Por-BzOH** monolayers on Si(100) at low surface concentrations are comparable to those observed for the **Por-BzSH** SAM on Au(111) ($t_{1/2} \approx 10$ s for both).[17]

(3) In the case of the **Fc-BzSH** monolayer on Au(111), the electron-transfer and charge-dissipation kinetics do not change substantially as a function of surface coverage: both rates remain fast as the coverage increases. This behavior is in contrast to that observed for both the **Fc-BzOH** and the **Por-BzOH** monolayers on Si(100) as well as that for the **Por-BzSH** SAM on Au(111).[17]

We advance two alternative explanations for the collective characteristics of the ferrocene and porphyrin monolayers on Si versus Au. In the first, the previously noted possibility that the strong covalent Si−O bond determines the orientation of the redox center with respect to the surface is invoked. If the molecular orientation dictates that all electronic communication between the redox center and the surface is mediated by the linker, that is, direct communication between the redox center and the surface does not occur, qualitatively similar electron-transfer and charge-dissipation behavior would be expected for the **Fc-BzOH** and **Por-BzOH** monolayers on Si(100), as observed. On the other hand, the much weaker and more malleable Au−S bond might not be the sole determinant of the molecular geometry. Instead, molecular packing could influence the detailed characteristics of the Au−S bond and, hence, the electronic coupling mediated through this linkage.[79] If the −BzS−Au linkage is affected by packing, these effects could be quite different for **Fc-BzSH** and **Por-BzSH** SAMs. In particular, the ferrocene unit is much smaller than the porphyrin and lacks the bulky mesityl groups (Chart 1). Regardless of the detailed nature of such effects, the observation of the very fast electron-transfer and charge-dissipation rates for the **Fc-BzSH** SAMs implies that the electronic coupling mediated by the −BzS− linker is relatively strong for these molecules. This view is consistent with previous studies of SAMs of other ferrocenes containing short aromatic and/or conjugating linkers.[34,35]

The second explanation expands on the idea of the adsorption geometry being the controlling factor in electron transfer and charge retention. For three out of the four cases studied here, the rates for both processes are similar and also vary with coverage in comparable fashion. In the case of the **Por-Bz** moiety, it does not much matter if the porphyrin is anchored in self-assembled layers of thiolates on Au or by covalent bonding via a Si−O linkage to Si. The unique behavior of the **Fc-BzSH** SAMs on Au may therefore be due to an additional, unique direct interaction between the ferrocene moiety and the metal surface that is afforded by the malleable Au−S bond and relatively short −BzS− linker. In this regard, direct adsorption of ferrocene to metals has been reported and has been shown to be reasonably strong.[65] In this picture, the ferrocene fragment may lie directly above the Au surface, in the same adsorption geometry regardless of coverage. This could explain both the very fast electron-transfer rates and the invariance of those rates with surface concentration. On the other hand, the porphyrin moiety in the **Por-BzSH** SAMs could not be brought into direct physical contact with the surface because the mesityl groups block this interaction and provide a degree of self-insulation.[17] Finally, we reiterate, however, that the very fast electron-transfer rates observed for the **Fc-BzSH** SAMs on Au(111) are unique only in the context of the present studies of the electroactive molecules on Si(100). A complete explanation for the different kinetic behavior of the different types of molecules on the different surfaces requires further studies in which the linker group and/or attaching atom(s) to the Si surface are varied.

V. Outlook

The general characteristics reported herein for the **Fc-BzOH** and **Por-BzOH** monolayers on Si(100) suggest that devices based on these architectures might favorably compete with current semiconductor devices. In particular, the state-of-the-art 256 MB dynamic random access memory (DRAM) cells use storage capacitors with an area of 5 μm^2 and a charge-storage capacity of 40 fF at 1.5 V.[80] The typical leakage current of these Si trench capacitors is ~1 fA, resulting in a charge-retention time of ~10 ms. Accordingly, the stored information must be frequently refreshed, at which times the memory cell is unavailable for other computations. This problem will only be exacerbated as the size of the semiconductor storage capacitor is diminished.

The results reported herein indicate that charge-retention times for the hybrid molecular/semiconductor constructs range from tens to hundreds of seconds, 3 to 4 orders of magnitude longer than that for a typical Si trench capacitor. In addition, the charge-storage capacity in a 5 μm^2 hybrid molecular/semiconductor architecture with a surface coverage of $\Gamma \approx 10^{-10}$ mol cm^{-2}

(79) Yaliraki, S. N.; Kemp, M.; Ratner, M. A. *J. Am. Chem. Soc.* **1999**, *121*, 3428−3434.

(80) Mandelman, J. A.; Dennard, R. H.; Bronner, G. B.; DeBrosse, J. K.; Divakaruni, R.; Li, Y.; Radens, C. J. *IBM J. Res. Dev.* **2002**, *46*, 187−212.

(which is readily achievable using our surface attachment protocol) is ∼500 fF, 10-fold larger than that of a Si trench capacitor. These figures only take into account the charge stored in the first redox state of the molecule in the monolayer. Porphyrin architectures with as many as eight redox states have been investigated on Au surfaces[16] and are currently being assembled on Si surfaces. The implementation of these molecular architectures in hybrid devices would greatly increase the amount of stored charge. Moreover, previous results from our laboratory have shown that the charge-retention characteristics of molecular-based information storage cells do not change as the size of the cell decreases,[10] further enhancing the potential performance of such memories as feature sizes shrink.

Finally, we note that the characteristics observed for prototypical **Fc-BzOH** and **Por-BzOH** monolayers on Si(100) investigated herein are not likely to represent the ultimate performance obtainable from a hybrid molecular/semiconductor device. Other linking atoms and organic linkers may further enhance the electron-transfer and/or charge-retention characteristics by modifying the electronic coupling with the surface.[79,81] Such studies are currently underway in our laboratories.

Acknowledgment. This work was supported by the DARPA Moletronics Program (MDA972-01-C-0072) and by ZettaCore, Inc. We thank S. E. Creager for making available the spreadsheet program for fitting the ratiometric AC voltammetric data.

Supporting Information Available: Experimental section describing the synthesis of **Fc-BzOH** and **Por-BzOH**; ^{1}H and LD-MS spectra for both compounds and their methyl benzoate precursors; ^{13}C NMR spectrum for the methyl benzoate precursor of **Fc-BzOH** (PDF). This material is available free of charge via the Internet at http://pubs.acs.org.

JA021169A

(81) Patrone, L.; Palacin, S.; Bourgoin, J. P.; Lagoute, J.; Zambelli, T.; Gauthier, S. *Chem. Phys.* **2002**, *281*, 325−332.